Performance Comparison of GPS Fault Detection and Isolation via Pseudorange Prediction Model based Test Statistics

Jangsik Yoo*, Jongsun Ahn*, Young Jae Lee* and Sangkyung Sung†

Abstract – Fault detection and isolation (FDI) algorithms provide fault monitoring methods in GPS measurement to isolate abnormal signals from the GPS satellites or the acquired signal in receiver. In order to monitor the occurred faults, FDI generates test statistics and decides the case that is beyond a designed threshold as a fault. For such problem of fault detection and isolation, this paper presents and evaluates position domain integrity monitoring methods by formulating various pseudorange prediction methods and investigating the resulting test statistics. In particular, precise measurements like carrier phase and Doppler rate are employed under the assumption of fault free carrier signal. The presented position domain algorithm contains the following process; first a common pseudorange prediction formula is defined with the proposed variations in pseudorange differential update. Next, a threshold computation is proposed with the test statistics distribution considering the elevation angle. Then, by examining the test statistics, fault detection and isolation is done for each satellite channel. To verify the performance, simulations using the presented fault detection methods are done for an ideal and real fault case, respectively.

Keywords: Fault detection and isolation, GPS, Pseudorange, Kalman filter, Test statistics

1. Introduction

Global Positioning System (GPS) has been applied in various industrial areas. For a reliable application, its accuracy, integrity, continuity, and availability have been addressed as critical issues. As a result, its application areas have been expanded, especially for aerial fields such as GPS applied to the takeoff and landing of aircraft. In this, an integrity that can correctly decide faulted status must be assured. In order to monitor the fault of GPS, both control station and user equipment monitor faults simultaneously. Currently, a control station receives information from 5 monitor stations over the world, and checks any fault from received satellites information to provide information to users through GIC (GPS Integrity Channel) [1, 2].

To monitor the fault of GPS, a user usually operates RAIM algorithm available for fault detection with a single GPS receiver only. Generally, RAIM can be divided into two types according to data processing class; a snapshot method and a method using past information [3]. A snapshot method performs fault detection using the measurement of a single epoch, and detects fault with redundant measurements. For such a method, the position comparison method and range comparison method proposed by Lee in the initial stage of RAIM research are representative ones [4]. In Brown and Hwang's method [5], they used past information as well, which examines fault at

† Corresponding Author: Department of Aerospace Information Engineering, Konkuk University, Korea (sksung@konkuk.ac.kr)
* Department of Aerospace Information Engineering, Konkuk University, Korea

a current time based on the verified past information. In addition, Da used the residual and covariance from the Kalman filter, and proposed a Chi-Square test method to monitor the fault in a GPS/INS integration system [9]. This method also monitors fault in current measurement based on verified past information. In general, the snapshot method is robust against continuous faults because it can be performed with only a single epoch measurement, yet it is limited in that the multiple faults detection is difficult because it is based on redundant measurements [17]. On contrast, the method using past information is vulnerable to continuous faults because it may use past information including faults that have been already occurred. It has an advantage over the multiple faults detection, however, because it can monitor the fault of an individual satellite.

In the initial stage of RAIM, various methods are developed, for example, least square, parity space, and range comparison method. They have been proven to have equivalent properties in integrity monitoring function [3]. Recently, on the other hand, in order to be applicable to the specific areas where high accuracy is required, the RAIM using carrier phase measurement has been investigated. In this respect, Lee proposed relative RAIM using carrier phase [6]. Relative RAIM calculates velocity during coasting interval by accumulating carrier phase, and applies it to the absolute RAIM algorithm for integrity verification. It then reflects such calculated velocity on the verified past position information through GIC to verify the integrity of current position information. One feature of relative RAIM is that it can solve the issue of Time to Alert (TTA) through the inherent RAIM concept. With the

differential of carrier phase, it could also solve the issue of integer ambiguity searching, and make the most benefit of the highly precise carrier phase at the same time. This method, however, has a limitation that it is only realized under the assumption that integrity information and carrier phase measurement are continuously received from GIC link. Besides, Feng implemented Carrier RAIM using carrier phase instead of pseudorange measurement from the existing RAIM method [7]. Carrier RAIM is applicable to the applied areas where a higher accuracy is required than the existing code-based RAIM. But it has a drawback since it is difficult to search the integer ambiguity in order to use the carrier phase information.

In contrast to this, this paper presents a position domain RAIM that can employ carrier phase update information without GIC link requirement. This is possible since the issue of integer ambiguity is resolved through a concept of carrier phase differential in the same manner as a relative RAIM, where it does not need to receive information from GIC. In detail, by projecting differentiated carrier phase on the line of sight vector, the proposed method computes the change of relative distance between satellite and receiver, and reflects such change on the verified past pseudorange measurement. Thus it predicts current pseudorange and uses it while calculating test statistics. Nevertheless, it should be noted that the fundamental assumption for the proposed carrier based method is that the carrier phase differential is free from fault with the help of lower level carrier signal integrity check process. Besides, this paper comparatively presents additional pseudorange prediction methods for position domain integrity monitoring including ephemeris differentials, the Kalman filter estimate using a second order pseudorange dynamic model, and the Doppler rate.

Meanwhile, in accordance with recent reinforcement of GNSS satellites such as the Galileo and GLONASS (GLObal Navigation Satellite System), an improvement in navigational performance is expected. The possibility of multiple faults becomes larger as more satellites become available. Studies regarding multiple faults have been actively progressed. Brown obtained change rate of position error (*SLOPE*) by using the size of the parity vector of an individual satellite [10]. Applying the parity space method, Brown found maximum value ($\max_{ij}(SLOPE_{max})$) among all visible satellites, and concluded that the identification of double faults is available. This method is used to find a set of satellites that maximizes the slope of position error over the size of parity vector during the selection of pairs from n visible satellites. It then makes a linear combination with each bias error. By recalculating $\max_{ij}(SLOPE_{max})$ in the pair of satellites, this method overcomes the issue of diminution effect in parity vector. However, there is one singularity issue since the case where the linear combination of bias in two satellites becomes '0' is unavoidable. In order to solve this issue in existing methods, Yoo proposed a method that

rearranges the parity conversion matrix into two portions, either suspected as fault composed by two satellites or not [11]. Similarly with Brown's method, this method was also proposed under the assumption of double faults only, thus cannot detect more general multiple faults case.

Unlike the previous position domain RAIM methods that check faults by constructing possible pairs with satellites where fault is suspected, the proposed method generates distinctively test statistics proportional to the faults of every satellite. Thus this automatically enables to monitor faults from multiple satellites signals. This paper is organized as follows; in Section 2, the position domain RAIM methods are presented by showing various pseudorange prediction models. In Section 3, it is provided detailed illustration to calculate the threshold for fault detection, which will be finally used to identify and isolate the fault signal. Section 4 includes the performance test of each prediction method with different fault cases. Finally, Section 5 contains the conclusion.

2. Pseudo Range Prediction Methods

In this paper, the integrity monitoring is considered in the application of air traffic control and management problem. Typically during aircraft cruise, a GPS satellite moves along the orbit and the distance changes because of the relative motion between the satellite and aircraft. Fig. 1 shows the distance change caused by the motion of a satellite and aircraft.
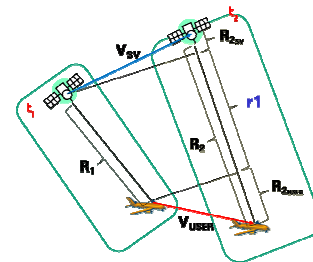

Fig. 1. Relative position change of satellite and aircraft.

In the figure, R_1 is the distance between satellite and aircraft at t_1; R_2 is the distance between satellite and aircraft at t_2; V_{SV} is the velocity vector of the satellite; V_{USER} is the velocity vector of aircraft; $R_{2_{SV}}$ is the change of relative range caused by the motion of satellite; $R_{2_{USER}}$ and is the change of relative range caused by the motion of the aircraft. In the figure, R_2 can be expressed as the sum of r_1, $R_{2_{SV}}$, and $R_{2_{USER}}$. $R_{2_{SV}}$ and $R_{2_{USER}}$ can be obtained by projecting each velocity vector on the line of sight vector at t_2. Several position update methods can be presented. For instance, as the value of the carrier phase differential means the distance change caused by the relative motion of a satellite and aircraft, it equals the sum of $R_{2_{SV}}$ and $R_{2_{USER}}$. Therefore, R_2, which is the

pseudorange at t_2, can be predicted as the sum of R_1, which is the pseudorange at t_1, and the carrier phase differential value from t_1 and t_2. Thus, assuming the availability of carrier phase differential, the predicted pseudorange for the *i*-th satellite in time t can be identified as following formula,

$$\hat{\rho}_{est,t,i} = \rho_{meas,t-1,i} + \Delta\Phi_{t,t-1,i} \tag{1}$$

where $\hat{\rho}_{est,t,i}$ is the predicted pseudorange for **i**th satellite in time t; $\rho_{meas,t-1,i}$ is the pseudorange measurement for the **i**th satellite in time $t-1$; and $\Delta\Phi_{t,t-1,i}$ is the carrier phase differential value for *i*-th satellite between time t and $t-1$. In the following process, the predicted pseudorange serves as the measurement vector in the navigation filter for residual and test statistics computation. Expanded from the suggested prediction formula in (1), this paper further discusses additional prediction methods using ephemeris with past GPS positional information, pseudorange estimate via second order dynamic model, and the Doppler rate. Similarly, each prediction method employs pseudorange update that can replace $\Delta\Phi_{t,t-1,i}$ in (1). In the following, each method is further described with its respective characteristics. For instance, the accuracy of the prediction using ephemeris and past GPS positional information primarily depends on the accuracy of position determination algorithm. Prediction method using the Doppler measurement is physically equivalent with the prediction using carrier phase differential value.

2.1 Prediction via ephemeris and past GPS position information

The position of satellite can be calculated through ephemeris data, and by differentiating it over time, V_{SV} in Fig. 1 can be obtained. The following equation identifies V_{SV}.

$$V_{SV,i,t_{1,2}} = P_{SV,i,t_2} - P_{SV,i,t_1} \tag{2}$$

where $V_{SV,i,t_{1,2}}$ is the velocity vector of **i**th satellite between t_1 and t_2; P_{SV,i,t_1} is the position vector of *i*th satellite in t_1; and P_{SV,i,t_2} is the position vector of ith satellite in t_2. Differentiating a single GPS position determination result over time allows V_{USER} can be calculated. Eq. (3) identifies V_{USER}.

$$V_{USER,t_{1,2}} = P_{USER,t_2} - P_{USER,t_1} \tag{3}$$

where $V_{USER,t_{1,2}}$ is user's velocity vector between t_1 and t_2; P_{USER,t_1} is user's position vector in t_1; and P_{USER,t_2} is user's position vector in t_2. The distance change can be calculated by multiplying $V_{SV,i,t_{1,2}}$ from (2) and $V_{USER,t_{1,2}}$ from (3) to the line of sight vector in t_2, respectively, and by adding them, as noted in the following.

$$\Delta r_{i,t_{1,2}} = G_{t_2} \cdot V_{SV,i,t_{1,2}} + G_{t_2} \cdot V_{USER,t_{1,2}} \tag{4}$$

where $\Delta r_{i,t_{1,2}}$ is the change of distance between **i**th satellite and user from t_1 to t_2; and G_{t_i} is the line of sight vector in t_2. Eq. (5) identifies the predicted pseudorange using update $\Delta r_{i,t_{1,2}}$ from (4).

$$\hat{\rho}_{est,t,i} = \rho_{meas,t-1,i} + \Delta r_{i,t_{1,2}} \tag{5}$$

where $\hat{\rho}_{est,t,i}$ is the predicted pseudorange for **i**th satellite in time t, and $\rho_{meas,t-1,i}$ is the pseudo range measurement for **i**th satellite in time $t-1$. The fault detection accuracy using the prediction equation in (5) highly depends on the positioning method at the current epoch, where standalone GPS or differential GPS positioning can be considered. In order to compare the fault detection performances for various prediction cases, individual test statistics are compared in chapter 4 for both the fault and fault free cases.

2.2 Prediction via code based pseudorange dynamic model

For the position domain RAIM, the pseudorange update can be accomplished through the Kalman filter estimate that provides the rate information of navigation data. This is acquired by modeling the pseudorange state with second order dynamics. Assumed with position rate and velocity rate, the following equation shows the dynamic model of predicted pseudorange.

$$\hat{\rho}_{est,t,i} = \rho_{meas,t-1,i} + v_{\rho,meas,t-1,i} \times dt + 0.5 \cdot \Delta v_{\rho,meas,t-1,i} \times dt^2 \tag{6}$$

where, $\hat{\rho}_{est,t,i}$ is the predicted pseudorange for the **i**th satellite in time t; $\rho_{meas,t-1,i}$ is the pseudo range measurement for the **i**th satellite in time $t-1$; $v_{\rho,meas,t-1,i}$ is the change of $\rho_{meas,t-1,i}$ over time; and $\Delta v_{\rho,meas,t-1,i}$ is the change of $v_{\rho,meas,t-1,i}$ over time. In formulating filter of pseudorange estimation, the state variables are defined as

$$x = [\rho_1, \dot{\rho}_1, \ddot{\rho}_1, \rho_2, \dot{\rho}_2, \ddot{\rho}_2, \cdots, \rho_n, \dot{\rho}_n, \ddot{\rho}_n]^T$$

and the measurement is $z = [\rho_1, \rho_2, \cdots, \rho_n]^T$, which is acquired from each satellite. Here, ρ_n in the state vectors is the pseudorange for *n*th satellite; $\dot{\rho}_n$ is the velocity component of a pseudorange for *n*th satellite; $\ddot{\rho}_n$ is the acceleration component of pseudo range for the *n*th satellite. Then the dynamic model for Kalman filter is represented by the following system and measurement model,

$$\begin{aligned} x_{k+1} &= Gx_k + w_k \\ z_k &= Hx_k + v_k \end{aligned} \tag{7}$$

where G and H is the state update matrix and measurement matrix, respectively, x_k is the state vector in time k, and z_k is the measurement in time k. It is assumed that the process noise, wk and the measurement noise, v_k follow the gaussian white noise distribution with covariance of Q_k and R_k, respectively. G and $\boldsymbol{H}$ are further described by

$$G = \begin{bmatrix} F_1 & O_{3\times3} & \cdots & O_{3\times3} \\ O_{3\times3} & F_1 & \cdots & O_{3\times3} \\ \vdots & \vdots & \ddots & O_{3\times3} \\ O_{3\times3} & O_{3\times3} & \cdots & F_1 \end{bmatrix}, \quad H = \begin{bmatrix} F_2 & O_{1\times3} & \cdots & O_{1\times3} \\ O_{1\times3} & F_2 & \cdots & O_{1\times3} \\ \vdots & \vdots & \ddots & O_{1\times3} \\ O_{1\times3} & O_{1\times3} & \cdots & F_2 \end{bmatrix}$$

where the sub-matrix F_1 and F_2 are given as follows

$$F_1 = \begin{bmatrix} 1 & dt & 0.5dt^2 \\ 0 & 1 & dt \\ 0 & 0 & 1 \end{bmatrix}, \quad F_2 = \begin{bmatrix} 1 & dt & 0.5dt^2 \end{bmatrix}$$

where the interval of epoch is defined as dt.

2.3 Prediction via the Doppler rate measurement

GPS satellite provides the measurement of Doppler shift to the user receiver. This measurement represents the Doppler shift caused by the relative motion of the satellite and receiver antenna. Theoretically, the Doppler measurement in a receiver can be computed from the PLL by counting the number of carrier phase cycles over a small time period divided by that time period. In practical implementation, the Doppler measurement additionally depends upon the receiver tracking loop bandwidth, i.e., the update rate of the tracking loop from which the Doppler is obtained. Thus according to the type of internal oscillator used, the resulting Doppler measurement will also vary in noise. Since the measurement inherently relies on the computation of the phase rate, noise characteristics are generally degraded than that of carrier phase signal [15, 16].

In the case of L1 frequency, the distance change caused by the Doppler effect can be obtained by multiplying the reference frequency with a wavelength of GPS carrier signal. The resulting Doppler rate can be represented as

$$D_{t,i} = f_{t,i} \cdot \lambda_{L1} = f_{t,i} \cdot c/f_{L1} \tag{8}$$

where $D_{t,i}$ is the Doppler rate of the *i*th satellite in time t; is the Doppler shift of the *i*th satellite in time t; c is velocity of light (299,792,458 m/s); f_{L1} is *L1* Carrier frequency (1575.42 MHz) and λ_{L1} is the wavelength of *L1* frequency (approximately 0.19m). Then the predicted pseudorange through the Doppler rate can be given as

$$\hat{\rho}_{est,t,i} = \rho_{meas,t-1,i} + D_{t,i} \times \Delta t \tag{9}$$

where, $\hat{\rho}_{est,t,i}$ is the predicted pseudorange for the *i*th satellite in time t; $\rho_{meas,t-1,i}$ is the pseudo range measurement for the *i*th satellite in time $t-1$; and $D_{t,i}$ is the Doppler data of the *i*th satellite in time t.

2.4 Prediction via the carrier differential method

Carrier phase data has an inherent advantage in that it contains much smaller measurement noise than the GPS code based pseudorange noise terms. In order to enable GPS pseudorange computed from carrier data, a preliminary determination of integer ambiguity is prerequisite. However, for simplicity, rather than fixing an absolute value for integer ambiguity resolution, only the carrier differential data with respect to each time epoch can be used for pseudorange prediction [12]. The predicted pseudorange is further processed for the calculation of test statistics of fault detection algorithm. Eq. (10) provides the predicted pseudorange in the current epoch by applying the carrier phase differential for the update of measured pseudorange in the previous epoch.

$$\hat{\rho}_{est,t,i} = \rho_{meas,t-1,i} + \left(\phi_t - \phi_{t-1} \right) \tag{10}$$

For the validation of the proposed pseudorange prediction method using carrier phase differential, it is assumed there is no fault on the acquired carrier information. For this, a fault detection algorithm to deal with a carrier signal fault needs to be implemented independently in conjunction with pseudorange prediction based methods. In conclusion, this section introduced four different pseudorange prediction methods, which are later used for calculating test statistics in fault detection problem.

2.5 Pseudorange prediction against slowly varying fault case

The fault in GPS measurement signal generally appears in an abrupt and short time period. An instant large fault can be detected by the pseudorange update in each consecutive epoch, but a slowly increasing small fault can be hardly detected in this mechanism. This is because the past measurement data contaminated with fault can be continuously used for the pseudorange prediction of (1) at the present epoch until a fault is finally determined by the threshold test. Therefore there may be significant latency to account for the accumulation of fault in test statistics, especially in case of slowly varying faults. To resolve this problem, this paper suggests the pseudorange differential updates be continuously accumulated in a proper window size, such that it can be used for the generation of test statistics of smooth fault cases. For instance, the accumulated carrier phase differential is used with the pre-defined prediction window size of *N*, as shown by.

$$\hat{\rho}_{est,t,i} = \rho_{meas,t-N,i} + \sum_{k=0}^{N-1} \Delta\Phi_{t-k,t-k-1,i} \qquad (11)$$

where, $\hat{\rho}_{est,t,i}$ is the predicted pseudorange for *i*th satellite; $\rho_{meas,t-N,i}$ is the pseudorange measurement for *i*th satellite in time *t-N*; $\Delta\Phi_{t-k,t-k-1,i}$ is the carrier phase differential value of *i*th satellite in time *t-k* and *t-k-1*. The window size *N* is statistically obtained considering the slope of practical faults. In implementing fault detection algorithm for both abrupt and slowly varying fault case, it is noted the generation of pseudorange prediction using Eq. (11) can be operated in a parallel way with the epoch-by-epoch prediction method.

3. Threshold for Fault Detection

In this section, a detailed illustration on the threshold computation for the proposed fault detection algorithms. First, to obtain the threshold of the fault detection algorithm, a certain assumption on the characteristics of the test statistics distribution is needed. In this paper, a general test statistics curve of zero mean, Gaussian distribution is employed. In practical application, however, due to the GPS satellite constellation characteristics, measurement noise tends to increase as the elevation angle of the satellite decreases in low range. As a result, when it is applied the same threshold in the overall elevation angle range may cause a wrong detection of 'False Alarm'. False alarm implies the case of wrong decision of fault occurrence even if the system has no fault occurred, which corresponds with the null hypothesis, type 1 error (α-error) in hypothesis testing. In the field of fault detection, this false alarm rate is defined by test operator and generally used as the detection threshold value.

In view of probability distribution, the false alarm rate matches with the tail areas of the probability distribution of the fault-free state. In this paper, as noted, a Gaussian distribution is used and the probability corresponding to the rate is used as the threshold, as shown in Fig. 2.
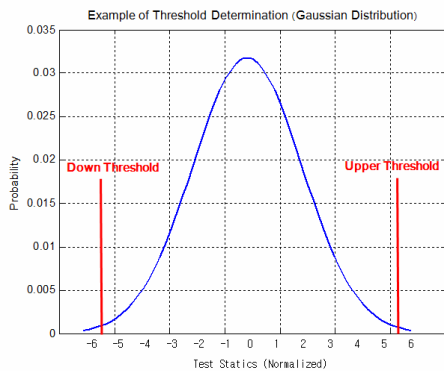
This paper presents a specific threshold determination algorithm that directly associates the elevation angle of each GPS satellite acquiring navigation data. This is because the elevation angle significantly affects the receiver error characteristics of GPS signal. For the meaningful classification, satellite elevation angle is divided by 10 degree intervals. Then the pseudorange error between the predicted one and the measured one is collectively drawn to provide a distribution of test statistics. Note that the distribution of test statistics are generated using the following equation

$$\Delta x_{t,i} = \hat{\rho}_{est,t,i} - \rho_{meas,t,i} \qquad (12)$$

where the $\Delta x_{t,i}$ represents the test statistics at time epoch t for the i-th satellite. By collecting a number of test statistics on the condition of fault-free measurements, the mean and variance of the distribution is computed for each interval statistically. Depending on this statistical value derived from normal condition, the criterion for fault detection is selected. In general integrity monitoring cases, the threshold in terms of elevation angle is typically computed using the following equation [12].

$$Threshold_{elevation} = \mu_{elevation} \pm 6 \times \sigma_{elevation} \qquad (13)$$

where $\mu_{elevation}$ is mean and $\sigma_{elevation}$ is standard deviation of the test statistics within the pre-defined elevation interval.

Fig. 3 shows the test statistics through the elevation angle ranges and the resulting upper threshold and lower threshold, where the threshold is determined using (13). For the simplicity of application, the interval of elevation angle is set to 10 degree. It is observed that the variance of test statistics strongly relies on the elevation angle.
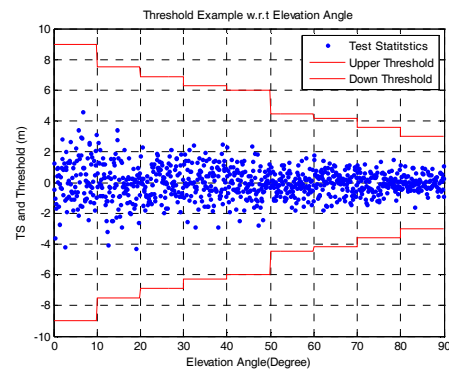

Fig. 3. Threshold determination with elevation angle.

The lowest threshold, which is measured at the interval of 80~90 degree, just equals one third of the highest threshold in elevation angle range below 10 degree. The most general threshold width is about 6 in between 40~50 degree range.
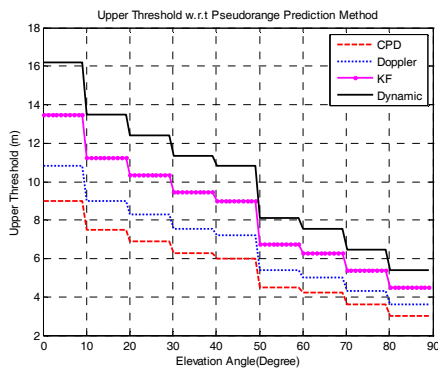

Fig. 2. Threshold determination using false alarm rate.

Fig. 4. Upper threshold with respect to various pseudo-range prediction methods.

Finally, Fig. 4 shows the respective threshold curves with respect to four different prediction methods for fault detection as presented in the previous section. Different threshold curves are calculated from respective test statistics variance characteristics of the proposed pseudorange prediction methods. It is clearly observed the threshold value decreases fast as the elevation angle increases. Specifically, the carrier phase differential (CPD) based prediction method provides the lowest threshold magnitude than other methods. This implies, given the same fault magnitude, CPD shows the highest detection alarm rate between test statistics and threshold. Doppler rate based prediction provides the second lowest threshold, thus a higher alarm rate is achieved than other methods except the carrier phase differential method. Then the computed threshold is used as the detection criterion in the following section.

4. Fault Models and Simulation Results

In this section, we first evaluate the estimation performance of the presented pseudorange prediction methods. In performance comparison, ideal fault and real fault cases are both considered.

First, to evaluate the performance of the presented methods, pseudorange prediction errors are compared together for the case without fault. The GPS data used for detection test is measured with 1 Hz update rate around the lakeside road at Ochang park, Chungbuk province. Fig. 5 shows the GPS satellite constellation and trajectory image. In Fig. 5(a) shows the mainly used satellite PRN2 is located around 20 degree elevation angle. Fig. 6 shows the pseudorange prediction error of each method, which is calculated based on the measurement when there is no fault.

In the figure, note that KF identifies the case using the second order pseudorange model; Dynamic identifies the case combining differential LOS vectors of user position and satellite position; Doppler identifies the case using

Doppler rate measurement; CPD identifies the case using carrier phase differential update. In the following numerical analysis, the update rate is 1 Hz, thus 1 epoch corresponds to 1 sec.

Observing Fig. 6, it is clear that the method using carrier phase differential outputs the smallest prediction error, which is followed by the methods using the Doppler, KF, and Dynamic LOS vector differential between user and satellite method, in order. It is illustrated that the method using Doppler or carrier phase differential value can provide relatively smaller range estimation error. Therefore it can be assumed that the two methods are better used for the generation of test statistics to determine fault detection. In the next section, an ideal fault model is examined to compare the detection performance of each method. Finally, considering statistical reliability, the prediction methods via Doppler and carrier phase differential methods are mainly examined to deal with the real fault case.
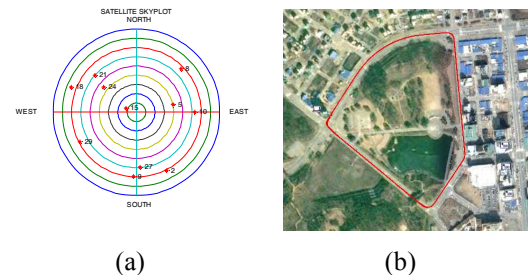

(a)   (b)

Fig. 5. (a) GPS satellites skyplot for dynamic data; (b) trajectory of dynamic data.
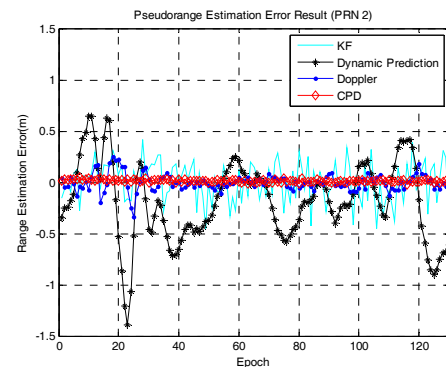

Fig. 6. Pseudorange prediction error using GPS dynamic data.

Observing Fig. 6, it is clear that the method using carrier phase differential outputs the smallest prediction error, which is followed by the methods using the Doppler, KF, and Dynamic LOS vector differential between user and satellite method, in order. It is illustrated that the method using Doppler or carrier phase differential value can provide relatively smaller range estimation error. Therefore it can be assumed that the two methods are better used for the generation of test statistics to determine fault detection. In the next section, an ideal fault model is examined to

compare the detection performance of each method. Finally, considering statistical reliability, the prediction methods via Doppler and carrier phase differential methods are mainly examined to deal with the real fault case.

4.1 Ideal fault model application results

For evaluating the FDI performance, simulation results under the ideal fault application case are illustrated. Fig. 7 shows fault models applied in the simulation. In the figure, two types of faults are applied with an impulse of 10m at 40 epoch instance and a bias of 10m during 10 epochs from 70 epoch instance. Random noise is added to the bias fault in a similar way as an actual fault. Then it is added to the fault-free pseudorange of the PRN 2 satellite.
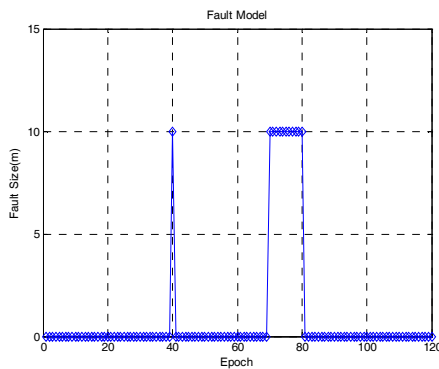

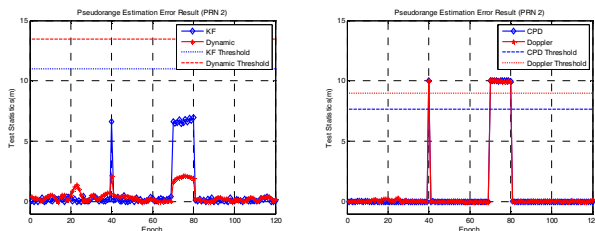**Fig. 7.** Fault model applied in the simulation.

Fig. 8. Comparison of test statistics for ideal fault case.

Fig. 8 shows the test statistics of the fault detection for four different methods. In the figure, CPD TS represents the test statistics for the method using the carrier phase differential and the Doppler TS represents the test statistics for the method using the Doppler rate measurement. Threshold represents the decision criterion of fault. Fault detection algorithm operates in both prediction methods of 1- epoch update model and N-epoch accumulation model, in a parallel way. Considering a normal ramp type fault case with 0.5 m/s slope and update rate of 1 sec, N is set to 20 in the simulation. In Fig. 8(a), as the test statistics of KF and Dynamic do not exceeds the threshold, thus cannot detect the applied faults in Fig. 7. Note that the elevation angle of the PRN2 is about 20 degree, thus the threshold of KF and Dynamic is larger than 10m. In contrast to this, CPD and Doppler method in Fig. 8(b) demonstrate

successful detection performance as the test statistics of both method exceed the threshold by 1m. In summary, the simulation result verifies that CPD and Doppler methods can detect faults, even if the GPS elevation angle is in low region, since the test statistics exceeds its corresponding threshold during the interval where each fault is applied. In the figure, the responses to impulse fault provide similar results in both methods. Yet, in bias fault case, it is found the method using the CPD calculates the test statistics more stably than the method using Doppler rate. This is because the pseudorange prediction error via carrier differential method is relatively smaller.

4.2 Real fault application results

In practical case, fault types of impulse and step function hardly occur. Thus a real fault example is adapted for assessing the performance of the proposed fault detection algorithm. Assumed that the KF and Dynamic cannot provide good performance against small fault values, only CPD and Doppler is considered. Fig. 9 shows partial result of the real fault example, which was observed during 2 hours and 40 minutes in Jan. 1 2004. Fault magnitude was obtained from satellite PRN 23. Partial intervals with only 20 epochs are representatively used to test the detection performance when the fault magnitude is very small. The curve fitted equation is given by (14) and drawn together with the original fault error values in Fig. 9.

$$Fault\ Model(t) = 2.884 \times 10^{-6} t^5 - 0.0004857 t^4$$
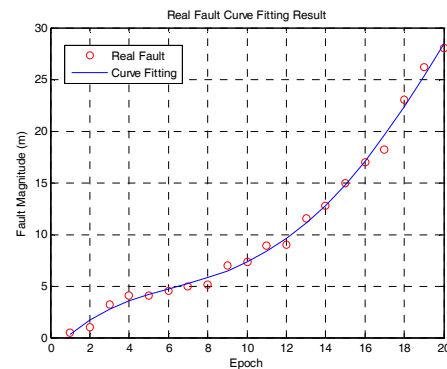$$+ 0.02209 t^3 - 0.3046 t^2 + 2.185 t - 1.599$$
$$(14)$$

Fig. 9. Real fault model observed from PRN 23 in Jan. 1 2004.

Using the real data with 20 epoch fault values as shown in Fig. 9, test statistics are calculated by the error between the predicted pseudorange and the measured faulty pseudorange using two prediction methods, i.e., Doppler and Carrier differential. Also detection algorithm operates via the prediction methods of N-epoch accumulation model with N = 20. Fig. 10 shows the test statistics against the

real fault case. Note that the elevation angle of PRN 2 is between 20deg and 30deg. In the figure, it is verified that fault can be detected via both methods. However, the detection time is different to each other; the Doppler method takes 11 epochs while the carrier phase differential method takes a shorter time of 10 epochs. As the threshold of the CPD method is smaller due to its stable test statistics property, detection time is relatively shorter than other methods.
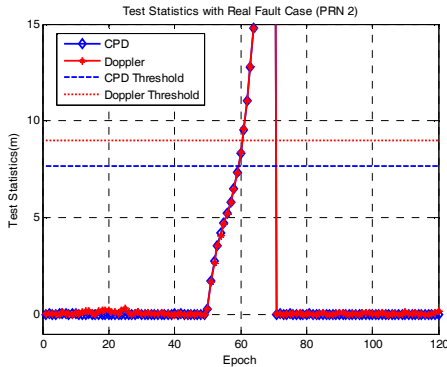

Fig. 10. Various test statistics comparison (real case).

Additional benefit from the proposed pseudorange prediction approach is that the isolation process is self-evident. This is because the test statistics in (12) contain the faulty PRN number in itself. Therefore when a fault is detected with the index of PRN number, it can be removed immediately in the positioning process, thus can suppress the position error divergence. Fig. 11 shows the fault isolation result, where it compares the 3 dimensional position error before and after the fault is isolated. Position calculated using fault free pseudorange data is assumed as the true value and the error result is plotted. As examined, carrier phase differential or Doppler rate is used for test statistics calculation. In the figure, it is observed that the position error due to the applied real fault can be apparently reduced through the presented fault isolation method. From epoch 50, the fault starts to affect positioning process and tends to increase error. As the fault
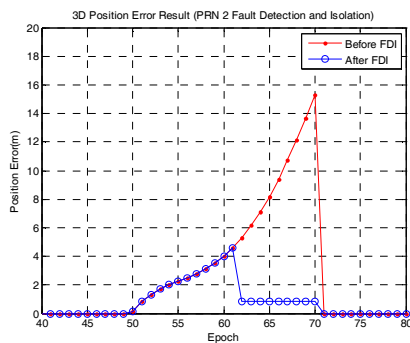
is detected via Doppler method at epoch 61 in Fig. 10, the error starts to decrease at epoch 62 by isolating the satellite of the corresponding PRN 2. Also with the proper threshold assignment of statistics, it is self evident that the fault isolation for double faults can be naturally achieved.

Table 1. Condition of GPS Fault Detection Algorithms

Experimental Spec.	Doppler	Carrier	Ahn	Lee
Receiver Type	Novatel OEM5			
Satellite Number	11		10	
HDOP/VDOP	1.2 / 1.5		1.1 / 1.6	
Data Sampling	1Hz			
Test Domain	Range		Position	

Table 2. Performance Comparison of GPS Fault Detection Algorithms

Fault Magnitude	Doppler	Carrier	Ahn	Lee
1m	X	X	X	X
3m	X	X	X	X
5m	Detected	Detected	X	X
7m	Detected	Detected	Detected	X

Finally, Table 1 and 2 present the performance comparison condition and results of the presented fault detection algorithms with the previous works [13, 14]. In Table 1, it is observed a similar condition on satellite availability and computation is arranged. When the detection algorithms are applied to GPS integrity monitoring for aircraft, its performance strongly depends on the position accuracy of aircraft and the overhead satellite constellation. Ahn presented a better result using a horizontal projection via residual vector [13], yet it could hardly identify the slowly varying fault with small magnitude of 5m as compared in the table. Comparatively, with the precise and secured carrier phase differential information, the presented detection method demonstrated an improved performance to detect small fault occurrence of 5m, as long as the soundness of the carrier data is allowed. Furthermore, with the help of the respective detection capability for each satellite channel, it is notable isolation for multiple faults case can be also achieved.

5. Conclusion

A GPS fault detection and isolation method based on the prediction of pseudorange is presented. For the pseudo-range prediction method, four different models are considered including the dynamics between user and satellite, pseudorange dynamic model, carrier phase differential data, and Doppler rate data. For the last two methods, it is assumed that the carrier signal from all available satellites is free from faults. Next, test statistics are calculated using the estimated position of each satellite,

Fig. 11. Comparison of errors before and after fault isolation (fault duration in 50 ~ 70 epoch).

and thus the pseudorange differential between the measured data and estimated data via the prediction models.

In order to compare the performance of the presented methods, a fault model with a combination of impulse and bias type fault, and real fault models with fault occurrence at the same time interval are introduced. When applying a single fault model, both methods using carrier phase differential and Doppler data detected both types of faults. However it was found that the method using carrier phase differential provided the fault identification test statistics more consistently than the method using Doppler data. And typically, test statistics using carrier phase differential has less accumulated errors than test statistics using Doppler measurement. Also the simulation result further verified that the proposed method could identify multiple faults from satellites with an arbitrary fault configuration.

Acknowledgements

References

[1] KwangHoon Kim, An Adaptive Filter Design for a Fault Tolerant Navigation System, Ph.D Dissertation, School of Electrical Engineering & Computer Science, Seoul National University, Feb. 2006.

[2] Pullen SP, Pervan BS, Parkinson BW, "A new approach to GPS integrity monitoring using prior probability models and optimal threshold search," PLANS '94, Las Vegas, NV, April 1994.

[3] EunSung Lee, Multiple Fault Detection and Isolation of GPS Carrier Measurement Using Array Antenna System, Ph.D Dissertation, Dept. of Aerospace Engineering, Konkuk University, Dec. 2004.

[4] YOUNG C. LEE, "Analysis of Range and Position Comparison Methods as a Means to Provide GPS Integrity in the User Receiver," Proceedings of the Institute of Navigation Forty-second Annual Meeting, June, 1986.

[5] Brown, R.G. and Hwang, P., "GPS Failure Detection by Autonomous Means within the Cockpit," Proceedings of the Annual Meeting of the ION, Seattle, WA, 24-26 June 1986.

[6] YOUNG C. LEE, "Position Domain Relative RAIM Method," Proceedings of the IEEE Position, Location, and Navigation Symposium (PLANS 2008), Monterey, CA, May 5-8, 2008.

[7] Feng S, Ochieng WY., Moore, T. Hill, C., and Hide, C., "Carrier Phase Based Integrity Monitoring for High Accuracy Positioning," GPS Solutions, 13 (1), pp.13-22.

[8] Li Jian, Liu Feng, Long Teng, "Study of Direct Acquisition of GPS P-code in Low-SNR," Proceedings of the 2008 Second International Symposium on Intelligent Information Technology Application, December, 2008.

[9] R. Da, "Faulure Detection of Dynamical Systems with the State Chi-Square Test," Journal of Guidance, Control, and Dynamics. Vol 17, No. 2, March-April 1994.

[10] R. Grover Brown, "Solution of the Two-Faulure GPS RAIM Problem Under Worst-Case Bias Conditions : Parity Space Approach," Journal of The ION, Vol. 44, No. 4, Winter 1997-1998, pp. 425~431.

[11] Chang Sun Yoo, Iee Ki Ahn, Sang Jeong Lee, "Two-Failure GPS RAIM by Parity Space Approach," Journal of Korean Society for Aeronautical & Space Sciences, Vol. 31, No. 6, Aug, 2003, pp. 52~60.

[12] Gang Xie, "Optimal On-Airport Monitoring of the Integrity of GPS-Based Landing Systems," Ph. D Thesis, 2004, Stanford University, pp 26~37.

[13] Yong-Woon Ahn, et. al., "The Abnormal Increasing Pseudorange Satellite Detection Method Using Comparison of Residual Horizontal Projection," Journal of The Korean Society for Aeronautical & Space Sciences, Vol. 38, No. 6, June 2010, pp. 570~576.

[14] Young C. Lee, "Analysis of Range and Position Comparison Method as a Means to Provide GPS Integrity in the User Receiver," Proceedings of the Annual Meeting of the Institute of Navigation, Seattle, Washington, June 1986.

[15] S. Ryan, G. Lachalelle and M.E. Cannon, "DGPS Kinematic Carrier Phase Signal Simulation Analysis in the Velocity Domain", Proceedings of ION GPS 97, September, 1997.

[16] Weidong Ding and Jinling Wang, "Precise Velocity Estimation with a Stand-Alone GPS Receiver," Journal of Navigation, Vol. 64, Issue 02, April 2011, pp 311~325.

[17] Jongsun Ahn, Rosihan, Dae Hee Won, Young Jae Lee, and Sangkyung Sung, "GPS Integrity Monitoring Method Using Auxiliary Nonlinear Filters with Log Likelihood Ratio Test Approach," Journal of Electrical Engineering and Technology, Vol6. No. 4, 2011, pp. 563-572.

Jangsik Yoo He received his B.S and M.S. degrees in Aerospace Information Engineering from Konkuk University, Korea, in 2009 and 2011, respectively. He is now a research staff in the Microinfinity Inc., Korea. His research interests include INS/GPS integrated navigation system, fault detection and isolation, and MEMS system.

Jongsun Ahn He obtained his B.S and M.S. degrees in 2007 and 2009, respectively. Currently, he is a Ph.D. candidate in the Department of Aerospace Information Engineering at Konkuk University. His research interests include Global Navigation Satellite Augmentation System (GNSS) and GPS signal fault detection.

Sankyung Sung He received his Ph.D. degrees in Electrical Engineering from Seoul National University, Korea, in 2003. Currently, he is an Associate Professor in the Department of Aerospace Information Engineering, Konkuk University. His research interests include inertial sensors, integrated navigation, and autonomous unmanned systems.

Young Jae Lee He is a Professor in the Department of Aerospace Information Engineering at Konkuk University, Korea. His research interests include integrity monitoring of GNSS signal, GBAS, RTK, attitude determination, orbit determination, and GNSS-related engineering problems.